Journal of Alzheimer's Disease 55 (2017) 343–358
DOI 10.3233/JAD-160327
IOS Press

Spatial Patterns of Longitudinal Gray Matter Change as Predictors of Concurrent Cognitive Decline in Amyloid Positive Healthy Subjects

Miguel Ángel Araque Caballero[a,*], Stefan Klöppel[b], Martin Dichgans[a,c], Michael Ewers[a] and for the Alzheimer's Disease Neuroimaging Initiative[1]
[a]*Institute for Stroke and Dementia Research, Klinikum der Universität München, Ludwig-Maximilians-Universität LMU, Munich, Germany*
[b]*Freiburg Brain Imaging, Departments of Neurology and Psychiatry, University Medical Center Freiburg, Freiburg, Germany*
[c]*Munich Cluster for Systems Neurology (SyNergy), Munich, Germany*

Handling Associate Editor: Natalie Marchant

Accepted 10 August 2016

Abstract. A substantial proportion of cognitively healthy elders (HC) show abnormally high amyloid-β (Aβ) deposition, a major pathology of Alzheimer's disease (AD). These subjects are at increased risk of Alzheimer's disease (AD) dementia, and biomarkers are needed to predict their cognitive deterioration. Here we used relevance vector regression (RVR), a pattern-recognition method, to predict concurrent cognitive decline on the basis of longitudinal gray matter (GM) changes, within two *a priori*, meta-analytically defined functional networks subserving episodic memory and executive function. Ninety-six HC subjects were assessed annually for three years with structural MRI and cognitive tests within the Alzheimer's Disease Neuroimaging Initiative. Presence of abnormal biomarker values of Aβ (Aβ+) were determined with cerebrospinal fluid and amyloid-PET (HC-Aβ+, $n = 30$; with $n = 66$ for normal HC-Aβ–). Using leave-one-out cross-validation, we found that in HC-Aβ+ patterns of GM changes within both networks predicted decline in episodic memory ($r = 0.61$, $p < 0.001$; $r = 0.40$, $p = 0.03$), but not executive function. In HC-Aβ–, GM changes within the executive function network predicted decline in executive function ($r = 0.44$, $p < 0.001$). Previously established region-of-interest (ROI)-based predictors such as changes in hippocampal volume, within an AD-signature multi-ROI, or total GM volume were not predictive of cognitive decline in any group or cognitive domain. RVR analyses unrestricted to the *a priori* networks yielded compatible results with the restricted case. In conclusion, RVR-derived patterns of subtle cortical GM changes are biomarker candidates of concurrent cognitive decline in aging and subjects at risk for AD.

Keywords: Aging, Alzheimer's disease, atrophy, gray matter, longitudinal, magnetic resonance imaging, multivariate, pattern recognition, relevance vector regression

*Correspondence to: Miguel Ángel Araque Caballero, Klinikum der Universität München, Institut für Schlaganfall- und Demenzforschung (ISD), Feodor-Lynen-Straße 17, 81377 München, Germany. Tel.: +49 89 4400 46159; Fax: +49 89 7095 8729; E-mail: miguel.caballero@med.uni-muenchen.de.

[1]Data used in preparation of this article were obtained from the Alzheimer's Disease Neuroimaging Initiative (ADNI) database (http://adni.loni.usc.edu). As such, the investigators within the ADNI contributed to the design and implementation of ADNI and/or provided data but did not participate in analysis or writing of this report. A complete listing of ADNI investigators can be found at: http://adni.loni.usc.edu/wp-content/uploads/how_to_apply/ADNI_Acknowledgement_List.pdf

INTRODUCTION

Abnormally high levels of brain amyloid-β (Aβ) in cognitively healthy elders (HC) are associated with an increased risk of developing Alzheimer's disease (AD) dementia [1–3]. An increase in Aβ alone is associated, however, with a relatively low rate of clinical worsening [4–6]. Instead, in HC subjects with abnormal levels of Aβ (HC Aβ+), cognitive decline [6, 7] and an increased risk of progression to mild cognitive impairment (MCI) or AD dementia [4, 5] are more strongly associated with increased levels of biomarkers of neurodegeneration (cerebrospinal fluid (CSF) tau, hippocampal volume, fluorodeoxyglucose (FDG)-positron emission tomography (PET) metabolism) than with the overall level of Aβ burden. In particular, changes in gray matter (GM) volume become apparent in close proximity to the first, preclinical changes in cognition [2], which suggests that the emergence of GM changes is a pivotal event in the early stages of AD.

Neuroimaging studies have shown that in HC Aβ+, GM volume changes are detectable widely throughout the brain, predominantly within the medial-temporal lobe [8–14], but also in other brain areas such as the medial prefrontal cortex and the parietal cortex [11, 14]. These results suggest that in HC Aβ+ subjects, GM atrophy emerges already in multiple brain areas. Those brain areas have previously been shown to support higher cognitive functions such as episodic memory and executive function, which are affected by aging and show accelerated decline early in the course of AD [4, 15, 16]. Thus, the assessment of such subtle but widespread GM changes may prove useful as a biomarker of concurrent cognitive decline in asymptomatic elderly subjects.

The aim of the current longitudinal study is to find patterns of GM atrophy that can be used to predict concurrent cognitive decline in two key cognitive domains (memory and executive function), in cognitively healthy subjects with and without abnormal levels of Aβ.

Here we used a pattern recognition method, called relevance vector regression (RVR), which allows the extraction of patterns within a high-dimensional feature space (e.g., voxel-based intensities representing local GM volume) for estimating continuous variables (e.g., cognitive test scores [17–19] or age [20, 21]). This is in contrast to other pattern recognition methods such as support vector machine (SVM) and Bayesian classifiers that have previously been applied to binary outcomes, such as classifying between normal subjects and subjects at risk for AD [22, 23], or between cognitively stable healthy elderly subjects, and subjects showing cognitive decline [24]. In recent cross-sectional studies using RVR, GM atrophy in the medial temporal lobe and other cortical brain areas was found to be a good predictor of accompanying global cognitive performance in a pooled sample of cognitively healthy elderly subjects, MCI, and AD [19] and within healthy subjects alone [17]. In the current longitudinal study in healthy subjects (HC Aβ–) and subjects at risk for AD (HC Aβ+), we applied RVR to predict concurrent decline in episodic memory and executive function on the basis of GM changes within functional networks known to subserve each of the cognitive domains. First, we used a cross-validation paradigm to establish patterns of GM changes within each network that are specific to at-risk subjects and healthy aging and that estimate changes in each specific cognitive domain. In addition, we compared the accuracy of the estimations resulting from the RVR with that of previously established region-of-interest (ROI)-based measures including changes in hippocampal volume, in multi-ROI GM volume within "AD-signature" regions [25] and in the whole GM. Finally, we computed unrestricted RVR analyses to assess whether GM changes outside of the *a priori* defined networks may also contribute to predict concurrent cognitive decline.

METHODS

Subjects

We included 96 cognitively healthy subjects from the Alzheimer's Disease Neuroimaging Initiative (ADNI) study [26]. In addition to the inclusion criteria defined by the ADNI study, the completion of baseline plus three yearly follow-up examinations, including structural magnetic resonance imaging (MRI) and neuropsychological assessments, was required in the current study. Moreover, the availability of a biomarker-based measurement of Aβ levels (CSF $A\beta_{1\text{-}42}$, Pittsburgh compound B (PiB)-PET, or AV-45 PET) at any time during their participation in ADNI was also required.

The diagnostic guidelines for the classification as HC within the ADNI study were as follows [27]: a baseline HC diagnosis was given if the patient had a clinical dementia rating (CDR) of 0 and Mini-Mental State Exam (MMSE) scores between 24 and 30 (inclusive), together with an absence of

memory complaints or impaired memory function. Normal memory function was defined according to the delayed Paragraph Recall subscale of the Wechsler Memory Scale – Revised, corrected for years of education: score ≥9 for 16 or more years of education, ≥5 for 8–15 years of education, and ≥3 for 0–7 years of education. See the ADNI Procedures Manual for details on diagnostic guidelines and neuropsychological examinations (available at the ADNI study website: http://adni.loni.usc.edu/wp-content/uploads/2010/09/ADNI_GeneralProcedures Manual.pdf).

As required by ADNI publishing guidelines, a description of the project's scope and purpose follows: The ADNI was launched in 2003 by the National Institute on Aging (NIA), the National Institute of Biomedical Imaging and Bioengineering (NIBIB), the Food and Drug Administration (FDA), private pharmaceutical companies and non-profit organizations as a $60 million, 5-year public-private partnership. The primary goal of ADNI has been to test whether serial MRI, PET, other biological markers, and clinical and neuropsychological assessment can be combined to measure the progression of MCI and early AD. Determination of sensitive and specific markers of very early AD progression is intended to aid researchers and clinicians to develop new treatments and monitor their effectiveness, as well as lessen the time and cost of clinical trials.

The Principal Investigator of this initiative is Michael W. Weiner, MD, VA Medical Center and University of California – San Francisco. ADNI is the result of efforts of many co- investigators from a broad range of academic institutions and private corporations, and subjects have been recruited from over 50 sites across the U.S. and Canada. The initial goal of ADNI was to recruit 800 subjects but ADNI has been followed by ADNI-GO and ADNI-2. To date these three protocols have recruited over 1,500 adults, ages 55 to 90, to participate in the research, consisting of cognitively normal older individuals, people with early or late MCI, and people with early AD. The follow up duration of each group is specified in the protocols for ADNI-1, ADNI-2, and ADNI-GO. Subjects originally recruited for ADNI-1 and ADNI-GO had the option to be followed in ADNI-2. For up-to-date information, see http://www.adni-info.org.

Cognitive assessments

Global cognitive performance was measured by the summary score of the Alzheimer's Disease Assessment Scale – Cognitive Subscale (ADAS-Cog) [28]. For the measure of multi-domain memory performance we used a previously established composite score, averaged across several memory tests (ADNI-MEM) [29]. Briefly, the ADNI-MEM score is based on Rey's Auditory Verbal Learning Test, the word recall tests from both the ADAS-Cog and MMSE assessments, and the Logical Memory test. Executive function was assessed with ADNI-EF [30], another composite score based on measures of Category Fluency (animals and vegetables), the Trail Making Tests A and B, Digit Span Backwards, Digit-Symbol Substitution, and Clock Drawing tests. Both ADNI-MEM and ADNI-EF are represented as z-scores.

CSF measurement of $A\beta_{1\text{-}42}$ levels

CSF samples were collected at multiple centers within the ADNI study, subsequently frozen at –80°C and sent for analysis to the ADNI Biomarker Core laboratory at the University of Pennsylvania. CSF $A\beta_{1\text{-}42}$ concentration was measured at baseline with the multiplex xMAP Luminex platform (Luminex Corp., Austin, TX) [31].

PiB-PET and AV-45-PET

PiB-PET scans were comprised of four 300-s frames taken 50 min after injection of 15 ± 1.5 mCi of (^{11}C) Pittsburgh compound B. CT or transmission scans were used for attenuation correction. The scans were preprocessed to result in standard orientation, voxel size, and resolution for all subjects. Here we used global standardized uptake value ratio (SUVR) PiB-PET values obtained as the average of fourteen representative ROIs distributed throughout the brain.

AV-45-PET scans consisted of four 300-s frames measured 50 min after injection of 10 ± 1.0 mCi of (^{18}F) Florbetapir. As with PiB-PET, we used SUVR AV-45-PET values obtained as the average of image values within several ROIs superimposed on images with standard orientation, voxel size, and resolution.

The PET Facility of the University of Pittsburgh carried out the preprocessing and analysis of the PiB-PET and AV-45 scans; thus the methodology, ROIs used for quantification and results of the analyses are all available at the ADNI study website (http://adni.loni.usc.edu/data-samples/pet/).

Dichotomization of diagnostic groups based on Aβ biomarker measurements

We divided the sample into groups of abnormally high Aβ levels (HC Aβ+) and normal Aβ levels (HC Aβ–) based on previously established cut-off values for CSF $A\beta_{1\text{-}42}$ concentration [31] (available in $n = 71$ subjects), and global brain levels of PiB-PET ($n = 5$) or AV-45 PET ($n = 20$) [32, 33]. That is, subjects with CSF $A\beta_{1\text{-}42}$ $\leq$192 pg/mL were classified as Aβ+ and for PiB-PET and AV-45-PET imaging, subjects with global SUVR values $\geq$1.5 and $\geq$1.13, respectively, were classified as Aβ+ (Table 1). This approach is supported by previous finding of good correspondence between the CSF measures of $A\beta_{1\text{-}42}$ and molecular PET for discriminating between elevated and normal levels [16, 33, 34].

These cut-off values were applied to the baseline values of the biomarker, in the case of CSF $A\beta_{1\text{-}42}$, but for PiB-PET and AV-45 PET, the baseline values had to be extrapolated during the ongoing study, as previously reported by our group [14] and others [8]. Briefly, in the ADNI I study, PiB-PET scans were obtained 12 to 48 months after baseline, and AV-45-PET 48 to 72 months. To estimate the Aβ status (Aβ+ versus Aβ–) at baseline, we used the following criteria: if the subject had more than one follow-up PiB-PET or AV-45 PET measurement available, we computed linear regressions with interval duration between visits as the predictor and global brain PiB-PET or AV-45-PET SUVR as the dependent variable. The intercepts of the regressions were taken as the PiB-PET and AV-45 SUVRs at baseline [35]. If a subject did not have follow-up measurements available but was below the cut-off value for the modality, it was considered Aβ– since amyloid deposition is expected to increase or remain stable in the age range of our subjects [10, 35]. If a subject did not have follow-up measurements available, but was above the cut-off value for the modality, the rate of change in PiB-PET and AV-45 PET was derived for the remainder of the ADNI HC cohort and the subject was extrapolated based on this annual rate.

Table 1
Subject characteristics at baseline

Group	HC Aβ+	HC Aβ–
N	30	66
Gender (f/m)	13/17	37/29
Age[a]	76.2 (5.3)	75.7 (5.2)
Years of education[a]	15.5 (3.2)	15.6 (3.0)
ADAS-Cog[a]	7.7 (3.3)*	5.7 (2.7)
ADNI-MEM ($\times 10^{-1}$)	8.0 (4.4)	9.0 (5.3)
ADNI-EF ($\times 10^{-1}$)	4.2 (6.2)*	7.6 (6.6)
ApoE ($\varepsilon 4+$ / $\varepsilon 4$–)	18/12**	9/57
Converters after 3/after 6 years[b]	4/12	2/14
Source of Aβ assessment		
CSF $A\beta_{1\text{-}42}$ (pg/mL)	138.1 (28.6)**	241.7 (28.3)
	$n = 22$	$n = 49$
PIB-PET (SUVR)[c]	1.58	1.39 (1.20–1.49)
	$n = 1$	$n = 4$
AV-45 PET (SUVR)[c]	1.33 (1.22–1.71)	1.02 (0.86–1.12)
	$n = 7$	$n = 13$

HC, healthy control; ADAS-Cog, Alzheimer's Disease Assessment Scale, Cognitive subscale; ADNI-EF, ADNI executive function Scale; ADNI-MEM, ADNI Memory Scale. [a]Values are mean (SD). [b]Number of subjects who converted from HC to MCI or AD, within 3/within 6 years after the initial visit. [c]Values are median (range). For PiB-PET and AV-45, the values of the first available measurement are shown. Here, statistical comparisons are not shown due to low number of subjects per cell. *$p < 0.05$; **$p < 0.001$.

3D T1-weighted MRI

The MRI scans were obtained from a pre-selection of ADNI I scans reported in [36]. This standardized dataset was proposed in order to consolidate selection criteria of MRI scans among researches accessing the ADNI database. The scans were all acquired in 1.5 T scanners and with $1.25 \times 1.25 \times 1.20\,mm^3$ voxel size. The scans passed image quality criteria established and preprocessed by the ADNI MRI Core, including field-gradient correction, B1-calibration correction and correction for residual intensity inhomogeneities with the N3 method. For the current study, only subjects with yearly follow-up visits for a total of 3 years were included (baseline plus three follow-ups) (http://adni.loni.usc.edu/data-samples/mri/).

Longitudinal pre-processing of MRI scans

The pre-processing pipeline used for the MRI scans has been previously described elsewhere [14], and has been used in previous voxel-based morphometry studies [37]. Briefly, for each subject, the MRI scans of each of the 4 time points (baseline and 3 annual follow-up scans) were rigidly aligned between time points and an intra-subject mean scan was obtained by averaging the realigned scans. The realigned MRI scans were segmented into GM, white matter (WM), and CSF [38]. The intra-subject mean image was normalized to the MNI T1-weighted MRI template via nonlinear diffeomorphic transformation (DARTEL tool in SPM8 [39]). Subsequently, the spatial normalization parameters computed for the mean image were applied to all image segments

(GM, WM, CSF) at each time point. The longitudinal pre-processing was performed with the VBM8 toolbox (http://dbm.neuro.uni-jena.de/vbm/ [37]) of SPM8 (http://www.fil.ion.ucl.ac.uk/spm/). The quality of the pre-processed scans was assessed visually. For the statistical analysis (see below), a GM mask was generated. All of the spatially normalized GM segments were summed voxel-by-voxel across subjects and time points. The resulting image was scaled to a maximum value of 1 and subsequently binarized, applying a threshold of >0.3.

Statistical analyses

Demographic differences

We tested for baseline group differences in age, gender, years of education, ApoE genotype ($\varepsilon 4$ carriers versus noncarriers), and cognitive test scores, as well as differences in the proportion of converters to MCI or AD within 3 and 6 years after baseline (see http://adni.loni.usc.edu/wp-content/uploads/2010/09/ADNI_GeneralProceduresManual.pdf for details on the MCI and AD diagnostic criteria). We computed *t*-tests for the continuous variables and χ^2 tests for the categorical variables. All statistical analyses were performed with the R statistical software, unless otherwise stated (http://www.r-project.com).

Differences in rates of cognitive change between Aβ groups

In order to assess the effect of high Aβ burden onto the rate of cognitive change, we performed a two-level statistical analysis. At the subject level, we computed rates of change in test score over the three years, for each test score and subject separately. At the group level of analysis, we formulated robust linear regression models for each test score with the rate of change in cognitive test score as main outcome and Aβ status as main predictor. We included age, gender, years of education, and test score at baseline as covariates. From this model, we obtained individual rates of change in each of the cognitive tests, adjusted by covariates. We aimed to predict these rates of change in test score, adjusted for covariates, with RVR and in ROI-analyses (see below).

Estimation of individual atrophy rates

We computed rates of change in GM volume, voxel-by-voxel and for each subject separately, by fitting a linear-regression model with time-after-baseline *t* (in years) as the only regressor [11, 14, 40]:

$$Y(t) = Bt + c \quad (1)$$

Y(t) represents the voxel-value of GM volume, *B* the rate of change and *c* a constant term. *B* is a 3D image with voxel values representing the average rate of GM change from baseline to the last visit. The rate-of-change images were smoothed with an isotropic Gaussian kernel of FWHM = 8 mm. The analysis was performed with SPM8 (http://www.fil.ion.ucl.ac.uk/spm/).

Differences in rates of GM atrophy between Aβ groups

We performed a voxel-wise multiple linear regression to assess the patterns of regional change in GM volume for each Aβ group separately, and the difference between said patterns. The main regressor was the group variable (HC Aβ– versus HC Aβ+) and the covariates were age, gender, years of education, and ApoE genotype (carriers of the $\varepsilon 4$ allele versus non-carriers). Unless otherwise stated, we applied a voxel-wise significance threshold of $\alpha = 0.001$ (uncorrected) and a cluster-size threshold, family-wise error corrected, of $\alpha = 0.05$ to correct for multiple comparisons. The analyses were performed with SPM8.

A priori defined cognitive networks

To restrict the search space of our main RVR analyses, we determined functional networks subserving executive function and episodic memory. These network maps were used in the RVR analysis (explained in the next section) as masks to restrict the voxels participating in the prediction of cognitive change.

The executive function network was obtained from a functional network map derived from resting-state fMRI by Smith et al. [41] (Supplementary Figure 1), and it comprises regions that were shown to be associated with executive function in a meta-analysis of task-fMRI activation studies. For episodic memory, no such resting-state functional network map was reported in that study [41]. Therefore, in order to obtain a map of the episodic memory network we directly used a meta-analytical approach based on the Neurosynth database (http://neurosynth.org) [42]. Neurosynth meta-analyses compute the likelihood that a certain brain region is associated with a specific cognitive function. This is done by computing, voxel by voxel, the ratio between the number of studies in the database that show activation in that voxel and report the specific cognitive function versus the number of studies that do not. This generates a z-scored

and FDR-corrected likelihood map of regions that are significantly associated with the cognitive domain in question. For determining regions representing episodic memory, we performed a search of the term "Memory Retrieval" as a proxy for episodic memory (Supplementary Figure 1).

Relevant vector regression

We used RVR to determine spatial patterns of GM volume change that are good estimators of cognitive change over 3 years. RVR was first proposed in [43] as a general method for machine learning, and was applied to neuroimaging only recently [18, 19]. Briefly, RVR is a kernel-based pattern recognition method formulated in a Bayesian framework. In RVR, a set of features, such as the voxel values coding the rate of change in GM volume, are used to calculate a kernel, which can be understood as a measure of similarity between features belonging to different subjects. Specifically, the kernel values are computed as the dot product between pairs of scans, which entails multiplying the scans voxel by voxel and summing up the result across voxels. In scans that exhibit similar patterns, i.e., similar atrophy rates in similar regions, the dot-product results in relatively high kernel values, whereas dissimilar patterns result in low kernel values. RVR assumes that a dependent variable (i.e., here the adjusted rates of change in cognitive test score) can be modeled as a linear combination (i.e., a weighted sum) of the kernel values. In our case, this means that RVR works under the assumption that there is a relationship between a particular pattern of GM volume change and cognitive change. More specifically, a step-wise optimization procedure (maximum-likelihood maximization) is used to find the weighted sum of kernel values that best estimates the actual rates of change in test score. During the optimization procedure, weighting values that contribute little to the estimation decrease exponentially in each step. Thus the estimated data points (rates of change in cognitive test score) are ultimately estimated only from a subset of relevant features from the full dataset.

Here, we computed one RVR models in each of the Aβ groups separately. For each group, the kernel values represented thus a measure of similarity between the patterns of GM volume change of the subjects in the group. For each model, a leave-one-out cross-validation (LOOCV) approach was used to estimate the (adjusted) rate of change in cognitive test score subject by subject, based on the regression weights estimated for all the subjects (the training set) except the one left out (the test set). Thus, LOOCV allowed us to estimate cognitive decline for each subject based only on the similarity of the subject's atrophy pattern with respect to the rest of its group. For each model, there were as many LOOCV steps as subjects in the group. As a measure of accuracy of the RVR predictions, we computed the Pearson moment correlation between the actual versus estimated rates of change in test score (i.e., across LOOCV steps).

Weight maps

For each LOOCV step, RVR can be used to obtain a spatial weight-map displaying the relative contribution of each voxel to the estimation of the rate of change for the subject left out. This is done by computing a weighted average of the GM volume change maps for all the subjects in the training set, where the weighting factors are the result of the RVR model (see previous paragraph). For each of the 6 RVR models, one average weight-map was calculated as the mean of the weight-maps across LOOCV steps. These final weight-maps were each z-score transformed, thresholded at $|z| > 1.5$, and overlaid onto an MNI T1 template separately, to represent regions maximally predictive of decline on the corresponding test score and group. This representation was chosen to highlight patterns of GM change within a group and consistent across subjects (LOOCV steps), but it has to be stressed than even voxels/regions below threshold do contribute to the RVR prediction. In addition, it has to be noted that even regions showing a relatively slow GM decline can appear in the weight map with high values, for example if decline in such regions is consistently found across subjects and if it consistently relates to cognitive decline across CV folds. All RVR analyses were performed with the PRONTO toolbox for SPM [44].

Cross-validation of RVR models

In both Aβ groups, we computed RVR analyses restricted to the episodic memory network to predict changes in memory performance (ADNI-MEM) and analyses restricted to the executive function network to predict changes in executive function (ADNI-EF). To assess the specificity of the patterns found in those analyses, we also computed RVR analyses crossing the cognitive networks with the cognitive tests: we predicted changes in ADNI-EF with RVR analyses restricted to the episodic memory network and vice versa. Finally, in order to assess whether regions outside of the *a priori* networks may have predictive value, we also computed unrestricted RVR analyses

applied to the whole GM, using no *a priori* networks. For unrestricted RVR, we also computed analyses to predict changes in global cognition as assessed by the ADAS-Cog test.

ROI-based analysis

To compare the performance of RVR with ROI-based approaches, we tested the predictive value of GM changes within three *a priori* selected ROIs: the hippocampus, the AD-signature multi-ROI presented in [45], and the whole GM. The hippocampus ROI was taken from the AAL Atlas [46], averaging left and right hippocampi. The AD-signature multi-ROI was comprised of the following regions from the AAL Atlas: medial temporal cortex, inferior temporal gyrus, temporal pole, angular gyrus, superior frontal gyrus, superior parietal lobule, supramarginal gyrus, precuneus, and inferior frontal sulcus (left and right averaged where applicable). For the whole GM ROI, the customized GM mask derived during scan pre-processing (see section *Longitudinal pre-processing of MRI scans* above) was used. The ROI-based rate of change in GM volume was computed as the average of the rates of change across all voxels with the ROI (see subsection *Estimation of individual atrophy rates*).

In linear regression models, we tested the predictive value of GM changes within each ROI when predicting the adjusted rates of change in test score for each of the cognitive measures (i.e., the same values as in RVR). As in RVR, we implemented a LOOCV procedure for each of the 6 linear regression models and computed the correlation between predicted and actual rates of change in test score across LOOCV steps, as well as the prediction error. For each model, there were as many LOOCV folds as subjects in the group. The linear models were computed with the lm function of the R statistical software and the LOOCV with the CVlm function of the DAAG package in R.

RESULTS

Sample description

HC Aβ+ had poorer baseline global cognition (ADAS-Cog, $p < 0.05$) and also poorer executive function (ADNI-EF, $p < 0.05$) than HC Aβ– subjects (Table 1). There was a higher proportion of ApoE ε4 carriers in the HC Aβ+ group when compared with the HC Aβ–. There were trend-level higher proportions of subjects who converted to either MCI or AD after 3 and after 6 years in the HC Aβ+ group when compared to HC Aβ–, but the differences were not significant ($p = 0.07$ and $p = 0.08$). There were no significant group differences in age, gender distribution, or years of education. The proportion of HC Aβ+ subjects as per AV-45 PET (35%) was similar to the proportion obtained with CSF $A\beta_{1\text{-}42}$ (31%, chi-square test $p > 0.5$), meaning that there was no bias toward Aβ+ classifications due to the later measurement of AV-45 PET with respect to CSF $A\beta_{1\text{-}42}$ (Table 1).

Aβ-group differences in cognitive decline over 3 years

For the rates of change in cognitive scores (Fig. 1, Table 2), HC Aβ+ subjects showed a faster

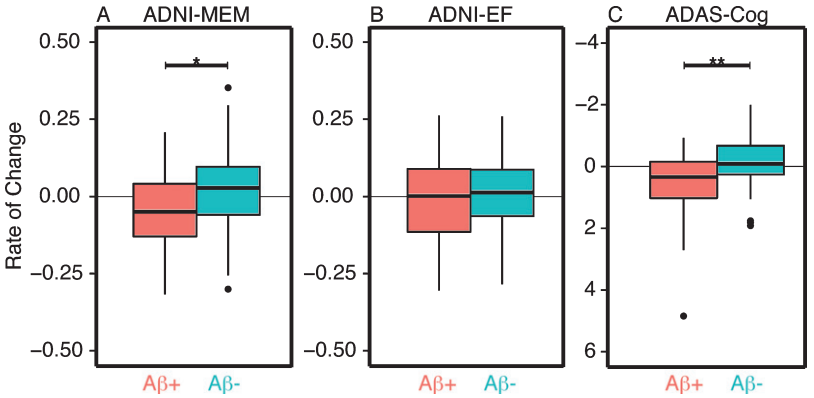

Fig. 1. Rates of change in the three cognitive test scores over 3 years, adjusted for age, gender, years of education and baseline test score. The boxes represent the inter-quartile ranges (IQRs) and the lines extend up to 1.5 times the IQR. The outliers are shown as points and are by definition outside the $\pm 1.5 \times$ IQR range. $^{*}p < 0.05$, $^{**}p < 0.001$.

Table 2
Results of regression analysis on group (HC Aβ– versus HC Aβ+) as main predictor of 3-year rates of change in cognition

Test	Predictor	Coefficient (SE)
ADAS-Cog	Aβ group ($\times 10^{-1}$)	6.4 (1.8)**
	Baseline-score ($\times 10^{-1}$)	–1.9 (0.3)**
	Age ($\times 10^{-2}$)	2.8 (1.6)*
ADNI-MEM	Aβ group ($\times 10^{-2}$)	–6.8 (2.8)*
	Baseline-score ($\times 10^{-2}$)	–4.2 (2.8)§
	Age ($\times 10^{-3}$)	–4.0 (2.5)§
ADNI-EF	Aβ group ($\times 10^{-2}$)	n.s.
	Baseline-score ($\times 10^{-2}$)	–4.3 (2.6)§
	Age ($\times 10^{-3}$)	–7.7 (2.9)*

HC, healthy control; ADAS-Cog, Alzheimer's Disease Assessment Scale, Cognitive subscale; ADNI-EF, ADNI executive function Scale; ADNI-MEM, ADNI Memory Scale. §$p < 0.1$; *$p < 0.05$; **$p < 0.001$.

decline than HC Aβ– in ADAS-Cog ($p < 0.001$) and ADNI-MEM ($p = 0.009$), but not in ADNI-EF when compared to HC Aβ–. Higher rates of decline were associated with higher age and lower baseline neuropsychological test score for ADAS-cog, and ADNI-EF (except for baseline score, $p = 0.05$), and at statistical trend level for ADNI-MEM (Table 2).

Aβ– group differences in GM change over 3 years

HC Aβ+ showed a distributed pattern of significant rates of GM atrophy, with the fastest rates (effect size $d > 1.5$) found in the hippocampus, caudate nucleus, and the temporal, pre-frontal, medial frontal, and medial parietal cortices (Fig. 2A). HC Aβ– showed significant rates of GM atrophy mainly within the prefrontal, cingulate, and temporal cortices, but to a much lower extent than HC Aβ– (Fig. 2B). When compared with HC Aβ–, HC Aβ+ showed faster rates of GM decline predominantly within the posterior hippocampus, posterior cingulate cortex, and precuneus (Fig. 3C).

Predictions of cognitive change from RVR restricted to the episodic memory network

When restricted to the episodic memory network, RVR yielded a pattern predictive of ADNI-MEM changes in the HC Aβ+ group ($r = 0.61$, $p < 0.001$, Fig. 3A). No pattern was obtained for changes in ADNI-MEM in HC Aβ– (Fig. 3B). In addition, no patterns predictive of ADNI-EF change were obtained for either group, indicating that the GM patterns detected by RVR within this network were specific to memory changes in the HC Aβ+ group. In contrast to RVR, the ROI-based analyses for hippocampus volume or whole GM volume yielded no significant estimations of change in ADNI-MEM score in HC Aβ+ (Hippocampus: $r = 0.27$, $p = 0.14$; whole GM: $r = 0.30$, $p = 0.11$), but showed a trend when the AD-signature was used as the predictor ($r = 0.35$, $p = 0.054$).

Predictions of cognitive change from RVR restricted to the executive function network

When restricted to the executive function network, RVR yielded a pattern predictive of ADNI-EF changes only in the HC Aβ– group ($r = 0.44$, $p < 0.001$, Fig. 4A). No pattern was obtained for changes in ADNI-EF in HC Aβ+. However, within this network RVR yielded a pattern predictive of ADNI-MEM changes in HC Aβ+ subjects ($r = 0.40$, $p = 0.03$, Fig. 4B). In contrast to RVR, none of the ROI-derived estimations of change in ADNI-EF for HC Aβ– was significant (Hippocampus: $r = –0.01$, $p = 0.94$; AD-Signature: $r = 0.19$, $p = 0.13$; whole GM: $r = 0.11$, $p = 0.34$).

Predictive patterns of GM change within the a priori networks

Figure 5A shows regions predictive of ADNI-MEM changes in HC Aβ+ for the RVR model restricted to the episodic memory network. The highest weights were found within the posterior hippocampi and medial-parietal regions. Figure 5B shows regions predictive of ADNI-MEM changes in HC Aβ+ for the RVR model restricted to the executive function network. In this case, the highest weights were found within the caudate nucleus and prefrontal regions, but also within medial-parietal regions, consistent with the previous result. Figure 5C shows the regions predictive of ADNI-EF changes in HC Aβ– when RVR was restricted to the executive function network. Regions with the highest weights were located in the putamen and frontal regions.

Predictions of cognitive change based on unrestricted RVR

In the unrestricted analyses, RVR yielded a pattern of GM changes that was associated with ADNI-MEM changes in HC Aβ+ ($r = 0.38$, $p = 0.037$, Fig. 6A), but not in HC Aβ– (Fig. 6B). Conversely, RVR yielded a pattern of GM changes that was associ-

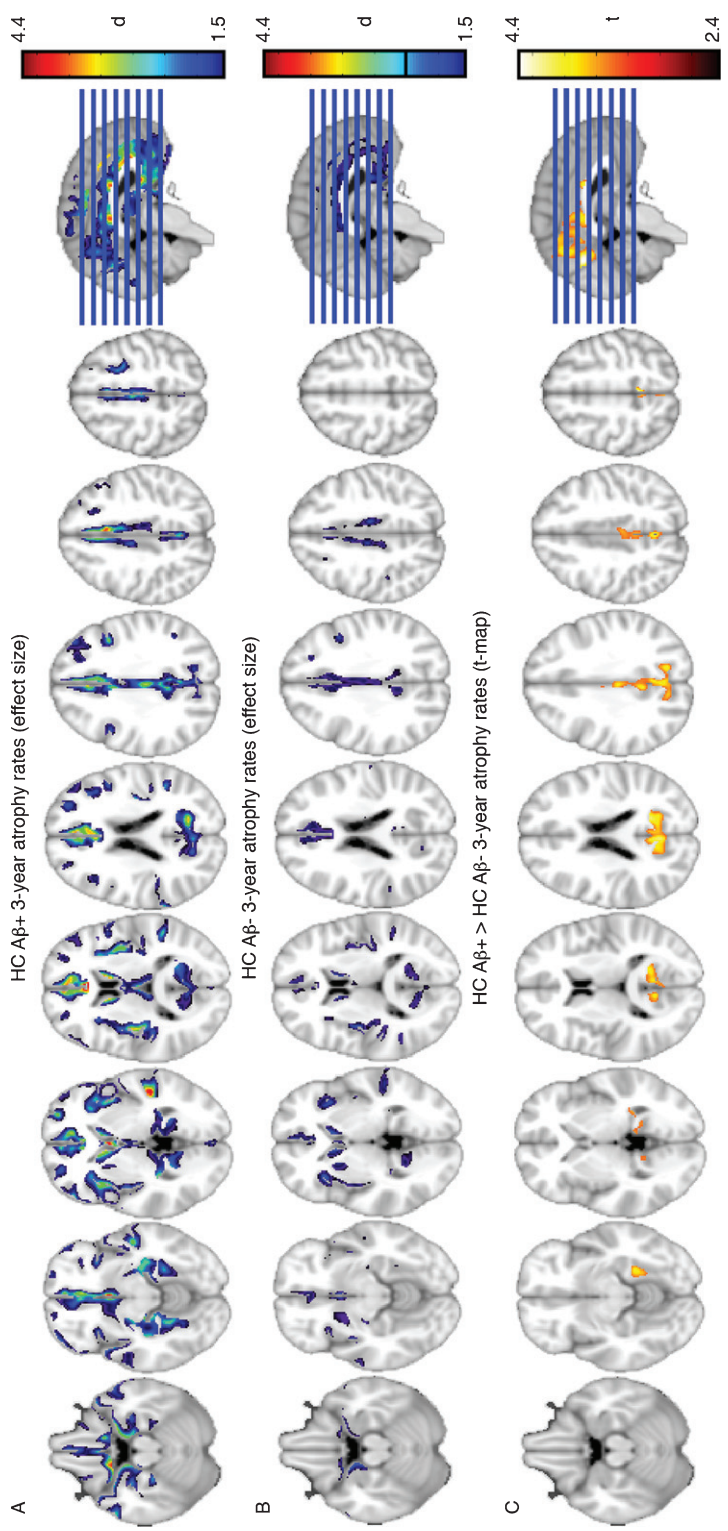

Fig. 2. Rates of change in GM volume over 3 years, adjusted for age, gender, years of education and ApoE genotype for HC Aβ+ (A), HC Aβ– (B), and statistical comparison between the two groups (C). Significance threshold for (A) and (B): voxel-wise $p = 0.001$ (uncorrected) and cluster-wise $p = 0.05$ (FWE-corrected). In addition, the maps are thresholded to show effect sizes $|d| > 1.5$ and represented in the same color scale to show the relative magnitude of the rates between the groups. The peak effect size for the HC Aβ+ was 4.4. The peak effect size for the HC Aβ– map is indicated in the color-scale of (B) and was 2.5. Significance threshold for (C): voxel-wise $p = 0.01$ (uncorrected) and cluster-wise $p = 0.05$ (FWE-corrected).

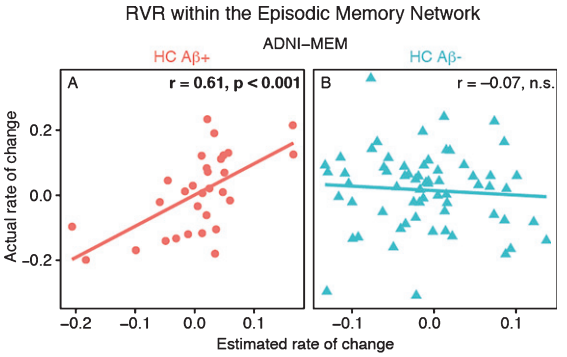

Fig. 3. Actual versus Estimated rates of change in test score resulting from the RVR models computed within the episodic memory network for ADNI-MEM in (A) HC Aβ+ and (B) HC Aβ– subjects.

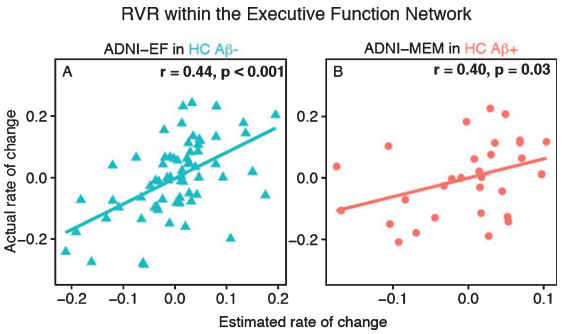

Fig. 4. Actual versus Estimated rates of change in test score resulting from the RVR models computed within the executive function network for (A) ADNI-EF in HC Aβ– and (B) ADNI-MEM in HC Aβ+ subjects.

ated with ADNI-EF changes in HC Aβ– ($r = 0.40$, $p = 0.006$, Fig. 6D), but not HC Aβ+ (Fig. 6C). In addition, no significant results were obtained for ADAS-Cog change ($r = 0.08$ for HC Aβ+ and $r = 0.10$ for HC Aβ–). The weight maps for the prediction of ADNI-MEM in HC Aβ+ and ADNI-EF in HC Aβ– are shown in Supplementary Figure 2 and a list of the regions with the highest weights in each map is shown in Supplementary Table 1.

DISCUSSION

Our main results showed that in HC Aβ+ subjects, RVR-derived patterns of GM volume change within *a priori* defined functional networks were good predictors of concurrent episodic memory decline. These patterns covered predominantly posterior parietal, hippocampal, and frontal brain regions and the method outperformed common neuroimaging markers such as changes in hippocampal volume. These results suggest that, in asymptomatic cognitively normal subjects at risk for AD, specific patterns of pronounced GM atrophy in functional network regions are associated with subtle decline in episodic memory. In contrast, in normal aging (HC Aβ–), frontal GM changes are predominantly associated with executive function.

In HC Aβ+ subjects, GM changes within the a priori, meta-analytically derived map of episodic memory network were highly predictive of concurrent decline in memory. Precisely these brain regions, i.e., the posterior parietal cortex and hippocampus, showed faster GM atrophy in HC Aβ+ compared to HC Aβ–. This is consistent with findings of faster GM volume decline within those regions, observed previously in HC Aβ+ subjects [8, 11, 14, 47] and to a larger extent in MCI due to AD [48, 49], which overall suggests that in HC Aβ+ early but subtle GM changes are found in key brain regions affected in AD. Thus, the RVR-derived weight maps provided anatomically feasible patterns of early GM change to track AD-related decline in episodic memory. Interestingly, also regions within the executive function network were predictors of concurrent decline in episodic memory in the HC Aβ+ subjects. Such association may be due to the fact that frontal brain regions, belonging to the executive function network, have a wider role in cognition, not restricted to a particular cognitive domain. That is, the frontal executive control regions are part of the fronto-parietal attention network, which plays an important role not only in executive function but also other cognitive abilities including episodic memory retrieval [42]. Thus, it is reasonable that GM changes in such frontal brain regions contribute to episodic memory changes in Aβ+.

Importantly, RVR yielded a better performance than region-based measures of GM change, such as the whole GM or the hippocampus, a region recommended as a marker of neurodegeneration in the early stages of pre-symptomatic AD by the NIA-AA diagnostic guidelines [1]. In addition, changes within a previously proposed multi-ROI measure of cortical GM, based on AD-signature regions [45], was only marginally associated with episodic memory changes in HC Aβ+. However, it should be noted that this signature was specifically tailored for the classification of HC Aβ+ versus healthy adults, and might therefore be suboptimal for the prediction of cognitive decline. Thus, our current results on RVR provide a novel,

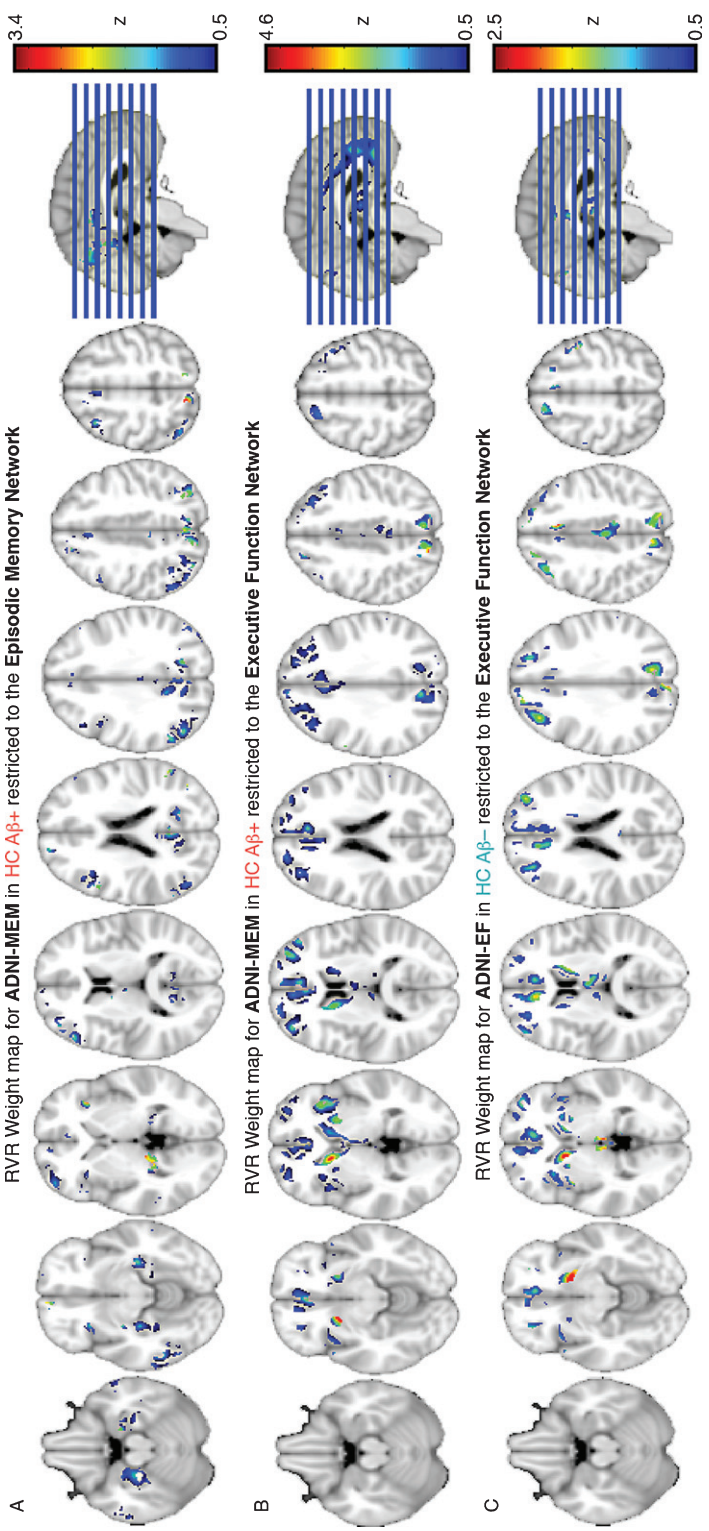

Fig. 5. Weight-maps showing regions in which GM volume change contributed significantly to predict concurrent change in (A) ADNI-MEM for HC Aβ+ in the episodic memory network, (B) ADNI-MEM for HC Aβ+ in the executive function network and (C) in ADNI-EF for HC Aβ− when restricted to the executive function network.

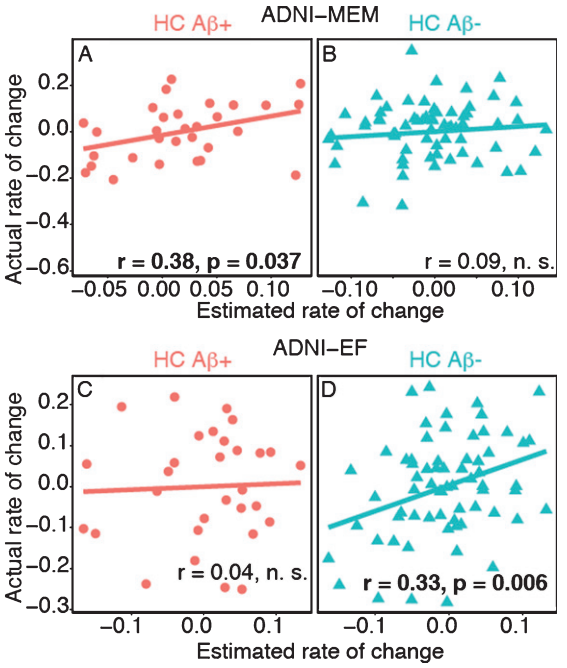

Fig. 6. Actual versus Estimated rates of change in test score resulting from the RVR models for ADNI-MEM (top row) and ADNI-EF (middle row) in HC Aβ+ (left column) and HC Aβ– subjects (right column).

promising approach to predict the rate of cognitive worsening in subjects at risk for AD.

In contrast to the findings in HC Aβ+, GM changes restricted to the executive function network in HC Aβ– subjects were good predictors of concurrent decline in executive function but not in memory. This pattern of GM changes was weighted towards the frontal lobes, consistent with previous findings showing that age-related frontal GM atrophy is associated with decline in executive function [50, 51] (reviewed in [52]). Together, our results suggest that RVR maps of GM changes show high sensitivity to track changes in episodic memory in HC Aβ+ in contrast to tracking changes in executive function in normal aging. However, sample size restrictions (see caveats below) should be kept in mind when interpreting the specificity of the findings, as it is possible to detect weaker ($r \sim 0.2$) but significant correlations with larger sample sizes.

The unrestricted RVR analysis, applied to the whole GM rather than restricted to *a priori* selected functional networks, was consistent with the restricted analysis in the sense that RVR yielded accurate estimations of ADNI-MEM changes in HC Aβ+ and ADNI-EF changes in HC Aβ–. However, these analyses resulted in a lower prediction accuracy, suggesting that core brain regions underlying episodic memory or executive function were already contained within the *a priori* functional network masks.

In contrast to the previous results, we found no association between GM change and global cognition as measured by ADAS-Cog in any of the groups. It is possible that global cognitive decline as assessed by ADAS-Cog is related to a diffuse pattern of GM changes that is hard to assess by RVR. Thus, the focus on specific cognitive domains by restricting the RVR analysis to the corresponding functional networks yielded a higher accuracy in predicting subtle concurrent cognitive decline.

Our current results extend previous applications of pattern recognition methods, such as SVM, which provide markers with clinically relevant accuracy for binary diagnostic classification (i.e., separating HC from AD subjects) [22, 24] or for the assessment of clinical outcome (e.g., conversion to AD) [22, 24, 53–55]. The application of pattern recognition methods has only recently been expanded for the estimation of continuous variables, made possible by the development of methods such as RVR [56]. RVR has been applied in neuroimaging for the prediction of illness severity in depression [57] and age in late adulthood [20, 21, 58]. For the estimation of cognitive performance, RVR has been previously tested in a pooled sample of HC, MCI and AD dementia subjects, cross-sectionally [19]. A pattern of GM differences predominantly within temporal and parietal brain regions was associated with global cognitive performance, with good estimation accuracy ($r = 0.58$). RVR yielded also a predictive model for episodic memory in the pooled sample, albeit at a lower level of accuracy ($r = 0.13$). However, the pattern of GM change associated with episodic memory was not reported, so that their findings cannot be directly compared with the current results. Together, ours and previous results suggest that RVR provides a promising approach to detect GM changes providing estimations of cognitive scores across the AD spectrum.

For the interpretation of the present study, some caveats need to be taken into account. First, our sample size was limited. The inclusion of longitudinal follow-up data of both MRI and cognition in a well-characterized cohort of cognitively healthy elderly with known Aβ status, however, is a strength of the study. We applied cross-validation to guard

against the influence of single observations, which may have a relatively higher weight in small samples. Moreover, it is worth noting that with relatively small sample sizes, higher correlation values between actual and predicted rates of change are required to reach significance. Conversely, with larger sample sizes, relatively lower correlation values may be deemed significant. This should be taken into account when interpreting the non-significant association between GM changes and episodic memory in HC Aβ– or executive function in HC Aβ+.

Second, our classification of Aβ status was based on different measures of amyloid deposition, namely CSF Aβ, PiB-PET, and AV-45 PET, which could have introduced measurement-specific bias in the classification. However, classifications of Aβ status based on AV-45 PET and CSF $A\beta_{1-42}$ yielded a similar proportion of Aβ+ subjects, suggesting that there was no measurement-dependent classification bias. In addition, the extrapolation of Aβ status from follow-up visits to baseline may have introduced a source of variability. However, all subjects assessed with amyloid-PET after baseline were, at the time of measurement, either well below or well above the corresponding cut-off values (Table 1), rendering thus unlikely that extrapolation may have introduced misclassifications.

Another caveat is that we focused solely on GM volume change, whereas a number of neurodegenerative processes such as brain hypometabolism, measured with FDG-PET, or WM disruption, assessed with diffusion MRI, may also contribute to cognitive decline in the preclinical stages of AD. A previous study in cognitively healthy elderly subjects showed that a combination of different imaging features (such as GM and WM volume, and FDG-PET) provided improved accuracy for the prediction of cognitive scores compared to each image modality alone [17]. Thus, a combination of different image modalities may also improve the accuracy of the prediction of cognitive decline in preclinical AD. However, any benefits for the improvement in predictive accuracy by the acquisition of additional measures must be weighted against the increase in stress for the patients, monetary costs, as well as feasibility in clinical practice. Finally, it has to be pointed out that we did not predict subsequent cognitive decline based on baseline GM atrophy, but rather estimated cognitive decline concurrent to the changes in GM. The present approach could be therefore used in clinical trials that include cognitively normal subjects at risk of AD, for instance to assess deviations from an expected course of cognitive decline given a certain pattern of GM changes. When using baseline maps as predictors of future cognitive decline no predictions were significant for any of the cognitive measures in either group (data not shown), which limits the current findings to longitudinal assessments of both GM and cognitive changes. Larger cross-sectional studies may however uncover cross-sectional GM differences that may have prognostic value for future cognitive decline.

In conclusion, our results highlight the value of RVR to predict concurrent cognitive decline on the basis of subtle neurodegeneration in preclinical AD and aging, when such GM changes may lie below the detection threshold for more traditional ROI-based methods.

ACKNOWLEDGMENTS

Dr. Dichgans received funding from the Alzheimer Forschung Initiative e.V. Dr. Ewers received support for this work from LMUexcellent and the European Commission (PCIG12-GA-2012-334259).

Authors' disclosures available online (http://j-alz.com/manuscript-disclosures/16-0327r1).

SUPPLEMENTARY MATERIAL

The supplementary material is available in the electronic version of this article: http://dx.doi.org/10.3233/JAD-160327.

REFERENCES

[1] Sperling RA, Aisen PS, Beckett LA, Bennett DA, Craft S, Fagan AM, Iwatsubo T, Jack CR Jr, Kaye J, Montine TJ, Park DC, Reiman EM, Rowe CC, Siemers E, Stern Y, Yaffe K, Carrillo MC, Thies B, Morrison-Bogorad M, Wagster MV, Phelps CH (2011) Toward defining the preclinical stages of Alzheimer's disease: Recommendations from the National Institute on Aging-Alzheimer's Association workgroups on diagnostic guidelines for Alzheimer's disease. *Alzheimers Dement* **7**, 280-292.

[2] Jack CR, Knopman DS, Jagust WJ, Petersen RC, Weiner MW, Aisen PS, Shaw LM, Vemuri P, Wiste HJ, Weigand SD, Lesnick TG, Pankratz VS, Donohue MC, Trojanowski JQ (2013) Tracking pathophysiological processes in Alzheimer's disease: An updated hypothetical model of dynamic biomarkers. *Lancet Neurol* **12**, 207-216.

[3] Dubois B, Hampel H, Feldman HH, Scheltens P, Aisen P, Andrieu S, Bakardjian H, Benali H, Bertram L, Blennow K, Broich K, Cavedo E, Crutch S, Dartigues JF, Duyck-

aerts C, Epelbaum S, Frisoni GB, Gauthier S, Genthon R, Gouw AA, Habert MO, Holtzman DM, Kivipelto M, Lista S, Molinuevo JL, O'Bryant SE, Rabinovici GD, Rowe C, Salloway S, Schneider LS, Sperling R, Teichmann M, Carrillo MC, Cummings J, Jack CR Jr (2016) Proceedings of the Meeting of the International Working Group (IWG) and the American Alzheimer's Association on The Preclinical State of AD; July 23, 2015; Washington DC, USA, Preclinical Alzheimer's disease: Definition, natural history, and diagnostic criteria. *Alzheimers Dement* **12**, 292-323.

[4] Vos SJ, Xiong C, Visser PJ, Jasielec MS, Hassenstab J, Grant EA, Cairns NJ, Morris JC, Holtzman DM, Fagan AM (2013) Preclinical Alzheimer's disease and its outcome: A longitudinal cohort study. *Lancet Neurol* **12**, 957-965.

[5] Knopman DS, Jack CR Jr, Wiste HJ, Weigand SD, Vemuri P, Lowe V, Kantarci K, Gunter JL, Senjem ML, Ivnik RJ, Roberts RO, Boeve BF, Petersen RC (2012) Short-term clinical outcomes for stages of NIA-AA preclinical Alzheimer disease. *Neurology* **78**, 1576-1582.

[6] Mormino EC, Betensky RA, Hedden T, Schultz AP, Amariglio RE, Rentz DM, Johnson KA, Sperling RA (2014) Synergistic effect of beta-amyloid and neurodegeneration on cognitive decline in clinically normal individuals. *JAMA Neurol* **71**, 1379-1385.

[7] Wirth M, Villeneuve S, Haase CM, Madison CM, Oh H, Landau SM, Rabinovici GD, Jagust WJ (2013) Associations between Alzheimer disease biomarkers, neurodegeneration, and cognition in cognitively normal older people. *JAMA Neurol* **70**, 1512-1519.

[8] Mattsson N, Insel PS, Nosheny R, Tosun D, Trojanowski JQ, Shaw LM, Jack CR Jr, Donohue MC, Weiner MW, Alzheimer's Disease Neuroimaging Initiative (2014) Emerging beta-amyloid pathology and accelerated cortical atrophy. *JAMA Neurol* **71**, 725-734.

[9] Nosheny RL, Insel PS, Truran D, Schuff N, Jack CR Jr, Aisen PS, Shaw LM, Trojanowski JQ, Weiner MW, Alzheimer's Disease Neuroimaging (2015) Variables associated with hippocampal atrophy rate in normal aging and mild cognitive impairment. *Neurobiol Aging* **36**, 273-282.

[10] Jack CR Jr, Wiste HJ, Weigand SD, Knopman DS, Lowe V, Vemuri P, Mielke MM, Jones DT, Senjem ML, Gunter JL, Gregg BE, Pankratz VS, Petersen RC (2013) Amyloid-first and neurodegeneration-first profiles characterize incident amyloid PET positivity. *Neurology* **81**, 1732-1740.

[11] Chetelat G, Villemagne VL, Villain N, Jones G, Ellis KA, Ames D, Martins RN, Masters CL, Rowe CC, AIBL Research Group (2012) Accelerated cortical atrophy in cognitively normal elderly with high beta-amyloid deposition. *Neurology* **78**, 477-484.

[12] Fjell AM, Walhovd KB, Fennema-Notestine C, McEvoy LK, Hagler DJ, Holland D, Blennow K, Brewer JB, Dale AM, Alzheimer's Disease Neuroimaging Initiative (2010) Brain atrophy in healthy aging is related to CSF levels of Abeta1-42. *Cereb Cortex* **20**, 2069-2079.

[13] Jack CR Jr, Wiste HJ, Knopman DS, Vemuri P, Mielke MM, Weigand SD, Senjem ML, Gunter JL, Lowe V, Gregg BE, Pankratz VS, Petersen RC (2014) Rates of beta-amyloid accumulation are independent of hippocampal neurodegeneration. *Neurology* **82**, 1605-1612.

[14] Araque Caballero MA, Brendel M, Delker A, Ren J, Rominger A, Bartenstein P, Dichgans M, Weiner MW, Ewers M, Alzheimer's Disease Neuroimaging Initiative (ADNI) (2015) Mapping 3-year changes in gray matter and metabolism in Abeta-positive nondemented subjects. *Neurobiol Aging* **36**, 2913-2924.

[15] Lim YY, Maruff P, Pietrzak RH, Ames D, Ellis KA, Harrington K, Lautenschlager NT, Szoeke C, Martins RN, Masters CL, Villemagne VL, Rowe CC, AIBL Research Group (2014) Effect of amyloid on memory and non-memory decline from preclinical to clinical Alzheimer's disease. *Brain* **137**(Pt 1), 221-231.

[16] Ewers M, Insel P, Jagust WJ, Shaw L, Trojanowski JJ, Aisen P, Petersen RC, Schuff N, Weiner MW (2012) Alzheimer's Disease Neuroimaging Initiative (ADNI), CSF biomarker and PIB-PET-derived beta-amyloid signature predicts metabolic, gray matter, and cognitive changes in nondemented subjects. *Cereb Cortex* **22**, 1993-2004.

[17] Wang Y, Goh JO, Resnick SM, Davatzikos C (2013) Imaging-based biomarkers of cognitive performance in older adults constructed via high-dimensional pattern regression applied to MRI and PET. *PLoS One* **8**, e85460.

[18] Chu C, Mourão-Miranda J, Chiu Y-C, Kriegeskorte N, Tan G, Ashburner J (2011) Utilizing temporal information in fMRI decoding: Classifier using kernel regression methods. *Neuroimage* **58**, 560-571.

[19] Stonnington CM, Chu C, Klöppel S, Jack CR, Ashburner J, Frackowiak RSJ (2010) Predicting clinical scores from magnetic resonance scans in Alzheimer's disease. *Neuroimage* **51**, 1405-1413.

[20] Gaser C, Franke K, Kloppel S, Koutsouleris N, Sauer H, Alzheimer's Disease Neuroimaging Initiative (2013) BrainAGE in mild cognitive impaired patients: Predicting the conversion to Alzheimer's disease. *PLoS One* **8**, e67346.

[21] Franke K, Ziegler G, Kloppel S, Gaser C (2010) Estimating the age of healthy subjects from T1-weighted MRI scans using kernel methods: Exploring the influence of various parameters. *Neuroimage* **50**, 883-892.

[22] Davatzikos C, Xu F, An Y, Fan Y, Resnick SM (2009) Longitudinal progression of Alzheimer's-like patterns of atrophy in normal older adults: The SPARE-AD index. *Brain* **132**, 2026-2035.

[23] Plant C, Teipel SJ, Oswald A, Bohm C, Meindl T, Mourao-Miranda J, Bokde AW, Hampel H, Ewers M (2010) Automated detection of brain atrophy patterns based on MRI for the prediction of Alzheimer's disease. *Neuroimage* **50**, 162-174.

[24] Clark VH, Resnick SM, Doshi J, Beason-Held LL, Zhou Y, Ferrucci L, Wong DF, Kraut MA, Davatzikos C (2012) Longitudinal imaging pattern analysis (SPARE-CD index) detects early structural and functional changes before cognitive decline in healthy older adults. *Neurobiol Aging* **33**, 2733-2745.

[25] Dickerson BC, Bakkour A, Salat DH, Feczko E, Pacheco J, Greve DN, Grodstein F, Wright CI, Blacker D, Rosas HD, Sperling RA, Atri A, Growdon JH, Hyman BT, Morris JC, Fischl B, Buckner RL (2009) The cortical signature of Alzheimer's disease: Regionally specific cortical thinning relates to symptom severity in very mild to mild AD dementia and is detectable in asymptomatic amyloid-positive individuals. *Cereb Cortex* **19**, 497-510.

[26] Mueller SG, Weiner MW, Thal LJ, Petersen RC, Jack C, Jagust W, Trojanowski JQ, Toga AW, Beckett L (2005) The Alzheimer's disease neuroimaging initiative. *Neuroimaging Clin N Am* **15**, 869-877, xi-xii.

[27] Petersen RC, Aisen PS, Beckett LA, Donohue MC, Gamst AC, Harvey DJ, Jack CR Jr, Jagust WJ, Shaw LM, Toga AW, Trojanowski JQ, Weiner MW (2010) Alzheimer's Disease

Neuroimaging Initiative (ADNI): Clinical characterization. *Neurology* **74**, 201-209.

[28] Rosen WG, Mohs RC, Davis KL (1984) A new rating scale for Alzheimer's disease. *Am J Psychiatry* **141**, 1356-1364.

[29] Crane PK, Carle A, Gibbons LE, Insel P, Mackin RS, Gross A, Jones RN, Mukherjee S, Curtis SM, Harvey D, Weiner M, Mungas D (2012) Development and assessment of a composite score for memory in the Alzheimer's Disease Neuroimaging Initiative (ADNI). *Brain Imaging Behav* **6**, 502-516.

[30] Gibbons LE, Carle AC, Mackin RS, Harvey D, Mukherjee S, Insel P, Curtis SM, Mungas D, Crane PK (2012) A composite score for executive functioning, validated in Alzheimer's Disease Neuroimaging Initiative (ADNI) participants with baseline mild cognitive impairment. *Brain Imaging Behav* **6**, 517-527.

[31] Shaw LM, Vanderstichele H, Knapik-Czajka M, Clark CM, Aisen PS, Petersen RC, Blennow K, Soares H, Simon A, Lewczuk P, Dean R, Siemers E, Potter W, Lee VM, Trojanowski JQ, Alzheimer's Disease Neuroimaging Initiative (2009) Cerebrospinal fluid biomarker signature in Alzheimer's disease neuroimaging initiative subjects. *Ann Neurol* **65**, 403-413.

[32] Jagust WJ, Bandy D, Chen K, Foster NL, Landau SM, Mathis CA, Price JC, Reiman EM, Skovronsky D, Koeppe RA, Alzheimer's Disease Neuroimaging Initiative (2010) The Alzheimer's Disease Neuroimaging Initiative positron emission tomography core. *Alzheimers Dement* **6**, 221-229.

[33] Landau SM, Breault C, Joshi AD, Pontecorvo M, Mathis CA, Jagust WJ, Mintun MA, Alzheimer's Disease Neuroimaging Initiative (2013) Amyloid-beta imaging with Pittsburgh compound B and florbetapir: Comparing radiotracers and quantification methods. *J Nucl Med* **54**, 70-77.

[34] Fagan AM, Mintun MA, Mach RH, Lee SY, Dence CS, Shah AR, LaRossa GN, Spinner ML, Klunk WE, Mathis CA, DeKosky ST, Morris JC, Holtzman DM (2006) Inverse relation between *in vivo* amyloid imaging load and cerebrospinal fluid Abeta42 in humans. *Ann Neurol* **59**, 512-519.

[35] Villemagne VL, Burnham S, Bourgeat P, Brown B, Ellis KA, Salvado O, Szoeke C, Macaulay SL, Martins R, Maruff P, Ames D, Rowe CC, Masters CL (2013) Amyloid β deposition, neurodegeneration, and cognitive decline in sporadic Alzheimer's disease: A prospective cohort study. *Lancet Neurol* **12**, 357-367.

[36] Wyman BT, Harvey DJ, Crawford K, Bernstein MA, Carmichael O, Cole PE, Crane PK, DeCarli C, Fox NC, Gunter JL, Hill D, Killiany RJ, Pachai C, Schwarz AJ, Schuff N, Senjem ML, Suhy J, Thompson PM, Weiner M, Jack CR, Jr, Alzheimer's Disease Neuroimaging Initiative (2013) Standardization of analysis sets for reporting results from ADNI MRI data. *Alzheimers Dement* **9**, 332-337.

[37] Luders E, Gaser C, Jancke L, Schlaug G (2004) A voxel-based approach to gray matter asymmetries. *Neuroimage* **22**, 656-664.

[38] Ashburner J, Friston KJ (2005) Unified segmentation. *Neuroimage* **26**, 839-851.

[39] Ashburner J (2007) A fast diffeomorphic image registration algorithm. *Neuroimage* **38**, 95-113.

[40] Dore V, Villemagne VL, Bourgeat P, Fripp J, Acosta O, Chetelat G, Zhou L, Martins R, Ellis KA, Masters CL, Ames D, Salvado O, Rowe CC (2013) Cross-sectional and longitudinal analysis of the relationship between Abeta deposition, cortical thickness, and memory in cognitively unimpaired individuals and in Alzheimer disease. *JAMA Neurol* **70**, 903-911.

[41] Smith SM, Fox PT, Miller KL, Glahn DC, Fox PM, Mackay CE, Filippini N, Watkins KE, Toro R, Laird AR, Beckmann CF (2009) Correspondence of the brain's functional architecture during activation and rest. *Proc Natl Acad Sci U S A* **106**, 13040-13045.

[42] Cole MW, Yarkoni T, Repovs G, Anticevic A, Braver TS (2012) Global connectivity of prefrontal cortex predicts cognitive control and intelligence. *J Neurosci* **32**, 8988-8999.

[43] Tipping ME (2001) Sparse Bayesian learning and the relevance vector machine. *J Mach Learn Res* **1**, 211-244.

[44] Schrouff J, Rosa MJ, Rondina JM, Marquand AF, Chu C, Ashburner J, Phillips C, Richiardi J, Mourao-Miranda J (2013) PRoNTo: Pattern recognition for neuroimaging toolbox. *Neuroinformatics* **11**, 319-337.

[45] Dickerson BC, Stoub TR, Shah RC, Sperling RA, Killiany RJ, Albert MS, Hyman BT, Blacker D, Detoledo-Morrell L (2011) Alzheimer-signature MRI biomarker predicts AD dementia in cognitively normal adults. *Neurology* **76**, 1395-1402.

[46] Tzourio-Mazoyer N, Landeau B, Papathanassiou D, Crivello F, Etard O, Delcroix N, Mazoyer B, Joliot M (2002) Automated anatomical labeling of activations in SPM using a macroscopic anatomical parcellation of the MNI MRI single-subject brain. *Neuroimage* **15**, 273-289.

[47] Oh H, Madison C, Villeneuve S, Markley C, Jagust WJ (2014) Association of gray matter atrophy with age, beta-amyloid, and cognition in aging. *Cereb Cortex* **24**, 1609-1618.

[48] Schuff N, Tosun D, Insel PS, Chiang GC, Truran D, Aisen PS, Jack CR, Weiner MW, Alzheimer's Disease Neuroimaging Initiative (2012) Nonlinear time course of brain volume loss in cognitively normal and impaired elders. *Neurobiol Aging* **33**, 845-855.

[49] La Joie R, Perrotin A, Barre L, Hommet C, Mezenge F, Ibazizene M, Camus V, Abbas A, Landeau B, Guilloteau D, de La Sayette V, Eustache F, Desgranges B, Chetelat G (2012) Region-specific hierarchy between atrophy, hypometabolism, and beta-amyloid (Abeta) load in Alzheimer's disease dementia. *J Neurosci* **32**, 16265-16273.

[50] Pfefferbaum A, Rohlfing T, Rosenbloom MJ, Chu W, Colrain IM, Sullivan EV (2013) Variation in longitudinal trajectories of regional brain volumes of healthy men and women (ages 10 to 85 years) measured with atlas-based parcellation of MRI. *Neuroimage* **65**, 176-193.

[51] DeCarli C, Massaro J, Harvey D, Hald J, Tullberg M, Au R, Beiser A, D'Agostino R, Wolf PA (2005) Measures of brain morphology and infarction in the framingham heart study: Establishing what is normal. *Neurobiol Aging* **26**, 491-510.

[52] Lockhart SN, DeCarli C (2014) Structural imaging measures of brain aging. *Neuropsychol Rev* **24**, 271-289.

[53] Toledo JB, Bjerke M, Chen K, Rozycki M, Jack CR Jr, Weiner MW, Arnold SE, Reiman EM, Davatzikos C, Shaw LM, Trojanowski JQ (2015) Alzheimer's Disease Neuroimaging Initiative, Memory, executive, and multidomain subtle cognitive impairment: Clinical and biomarker findings. *Neurology* **85**, 144-153.

[54] Peter J, Scheef L, Abdulkadir A, Boecker H, Heneka M, Wagner M, Koppara A, Klöppel S, Jessen F (2014) Gray matter atrophy pattern in elderly with subjective memory impairment. *Alzheimers Dement* **10**, 99-108.

[55] Shaffer JL, Petrella JR, Sheldon FC, Choudhury KR, Calhoun VD, Coleman RE, Doraiswamy PM (2013) Predicting cognitive decline in subjects at risk for Alzheimer disease by using combined cerebrospinal fluid, MR imaging, and PET biomarkers. *Radiology* **266**, 583-591.

[56] Tipping M (2000) The relevance vector machine. In *Advances in Neural Information Processing Systems*, Solla SA, Leen TK, Müller K-R, eds. MIT Press, Cambridge, MA, pp. 652-658.

[57] Mwangi B, Matthews K, Steele JD (2012) Prediction of illness severity in patients with major depression using structural MR brain scans. *J Magn Reson Imaging* **35**, 64-71.

[58] Mwangi B, Hasan KM, Soares JC (2013) Prediction of individual subject's age across the human lifespan using diffusion tensor imaging: A machine learning approach. *Neuroimage* **75**, 58-67.